NUMERICAL HEAT TRANSFER MODEL FOR FROST PROTECTION OF CITRUS FRUITS BY WATER FROM A SPRAYING SYSTEM

by

Roy J. ISSA

Department of Engineering and Computer Science, Mechanical Engineering Division,
West Texas A&M University, Canyon, Tex., USA

Original scientific paper
DOI: 10.2298/TSCI110331084I

A simplified model is developed to simulate the conditions associated with the protection of fruits from frost damage using water from a spraying system. The model simulates the movement of the solidifying water front on a single fruit, and based on that determines the spray frequency needed for a water film to continuously surround the ice-coated fruit to prevent the fruit temperature from dropping below 0 °C. Simulations are presented for the frost protection of sweet oranges (citrus sinensis). The effect of environmental conditions such as air temperature, air velocity, surface radiation, and water film evaporation on the development of the ice layer encasing is considered. Simulations show the effect the encasing ice sheet thickness has on the fruit temperature if water from a spraying system is turned off permanently. Experimental tests are also conducted to determine the change in the thermal properties of citrus sinensis for operating temperatures that range from above freezing to sub-freezing. The results of the experimental tests and the numerical simulations shall lead to a better understanding of fruit protection from frost damage by the application of water from a spraying system.

Key words: *heat transfer, ice, citrus sinensis, thermal property tests*

Introduction

For the last several years, water spraying of fruits has been shown to be very effective in the protection of fruits from frost damage. At near freezing or sub-freezing temperatures, water sprayed on fruits from a water sprinkler system results in an ice layer that encases the surface of the fruit and protects it from frost damage. When water at 0 °C changes to ice at 0 °C, 333.7 kJ per kg is released to the ambient at atmospheric pressure. The fruit temperature remains at 0 °C as long as the liquid and solid phase coexist together. Since ice has much higher thermal conductivity than liquid water, the temperature of the encased fruit quickly reaches the freezing temperature of water. Fruits have high sugar contents and they tend to freeze at temperatures lower than that of pure water. In order for the temperature of the encasing ice and the fruit not to drop below 0 °C, a water film must continuously surround the ice-coated fruit. However, excessive ice buildup has detrimental effect due to the damage it can cause to the fruit.

* Author's e-mail: rissa@mail.wtamu.edu

Several researchers have conducted studies over the years on water spraying of fruits for frost protection. In many of these studies, the rate of water application was determined from an energy balance on the targeted plants or fruits. Lengerke [1] conducted studies on frost protection of tea plants (camellia sinensis) by spraying water. His studies show this method to be a promising alternative to other practical methods such as artificial fogs, wind machines and heating. Hamer [2-4] used an automated sprinkler with a variable irrigation rate to protect apple fruit buds and flowers from freezing temperatures. The spray system was turned on when the bud temperatures fell below a critical temperature level. Edling *et al.* [5] applied water on citrus tree trunks and branches using micro-sprinklers that used lower flow rates than conventional sprinkler systems. Anconelli *et al.* [6] used micro-sprinklers and micro-sprayers at ground level with different characteristics and flow rates in protecting fruit orchards from frost. A better performance from micro-sprinklers with respect to micro-sprayers was observed. Also, micro-sprinklers performed better at higher flow rates. Ghaemi *et al.* [7] used an over-tree sprinkler system to protect peach and orange blossoms from frost damage. Similar studies were also conducted by Stombaugh *et al.* [8] for frost protection of strawberries.

From review of literature, limited experimental or numerical heat transfer studies have been done on the protection of citrus fruits from frost damage. Furthermore, the research conducted by all these researchers did not consider the dependency of the spray frequency on the time it takes for the water film surrounding the fruit surface to freeze. The amount of water spray needed can be further optimized. The purpose of this study is to experimentally determine the effect ambient temperature has on the thermal properties of sweet orange (*citrus sinensis*) for temperatures ranging from above freezing to sub-freezing. A numerical model is developed to simulate the effect of environmental conditions such as air temperature, air velocity, surface radiation and water film evaporation on the development of the ice layer encasing the fruit surface. Numerical simulations show the effect the ice sheet thickness has on the fruit temperature if the water spray system is turned off permanently.

Theoretical approach

Forced convection over a sphere

In the development of the numerical model for the frost protection of citrus fruits, the geometry of the fruit is considered spherical. Several experimental studies have been conducted in the past by various researchers [9-11] to investigate the local heat transfer coefficient for forced flow over spheres. Experimental data gathered from the review of these studies is compiled and is shown in figs. 1 and 2 for the flow over the forward and aft region of a sphere. Based on the review of literature, the following empirical correlations are obtained for the Nusselt number for forced flow over a sphere as function of the angular displacement from the stagnation point, θ:

(1) For $0 < \theta < 105°$ (forward region of a sphere)

$$\ln\left(\frac{\mathrm{Re}^{0.65}}{\mathrm{Nu}}\right) = 1.396\cdot 10^{-4}\theta^2 - 2.423\cdot 10^{-3}\theta + 1.531 \tag{1}$$

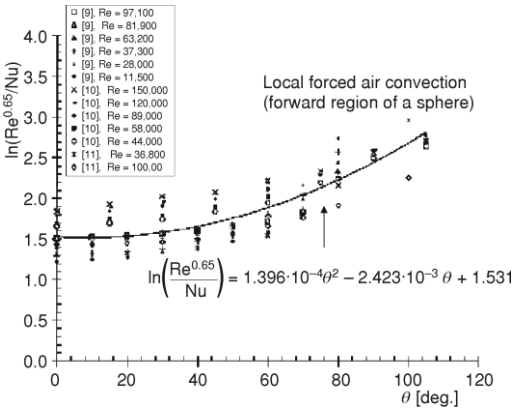

Figure 1. Local forced air Nusselt number for the forward region of a sphere

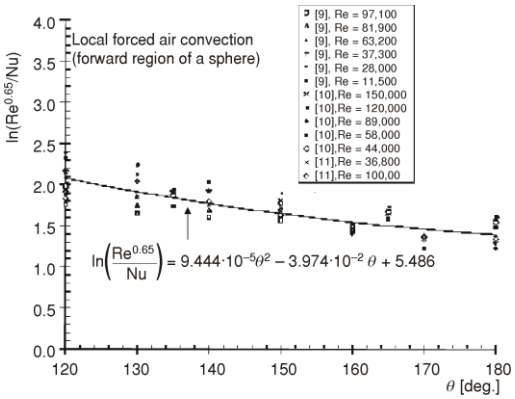

Figure 2. Local forced air Nusselt number for the aft region of a sphere

(2) For $120^{o} < \theta < 360°$ (aft region of a sphere)

$$\ln\left(\frac{\mathrm{Re}^{0.65}}{\mathrm{Nu}}\right) = 9.444\cdot10^{-5}\theta^{2} - 3.974\cdot10^{-2}\theta + 5.486 \tag{2}$$

Empirical correlations (1) nad (2) are valid for flow Reynolds numbers that range from $1.15\cdot10^{4}$ to $1.5\cdot10^{5}$. The Nusselt number used in the simulation study (presented in this paper) is the average Nusselt number obtained along the circumference of the fruit spherical surface. The average heat transfer coefficient for the air flow over the sphere, h_{g}, can then be shown as:

$$h_{\mathrm{g}} = 0.1513\frac{k_{\mathrm{g}}}{D_{\mathrm{o}}}\left(\frac{U_{\mathrm{g}}D_{\mathrm{o}}}{\nu_{\mathrm{g}}}\right)^{0.65} \tag{3}$$

Energy balance on a solidifying water front

Heat transfer by conduction through the ice layer developed on the outer surface of a solid spherical fruit, q_{s}, is balanced by heat transfer due to water evaporation, forced convection and radiation at the outer surface of the ice layer (fig. 3). Using thermal resistor approach, this heat transfer is expressed as:

$$q_{\mathrm{s}} = \frac{T_{\mathrm{s,H_2O}} - T_{\infty}}{R_{\mathrm{cond}} + \dfrac{1}{\dfrac{1}{R_{\mathrm{conv}}} + \dfrac{1}{R_{\mathrm{rad}}} + \dfrac{1}{R_{\mathrm{evap}}}}} \tag{4}$$

Heat transfer from the solidifying water on the outer surface of the sphere can also be expressed as function of the speed of the moving ice front, dx/dt, and the latent heat of fusion for water, $h_{\mathrm{sl,H_2O}}$:

$$q_{\mathrm{s}} = 4\pi(r_{\mathrm{o}} - x)^2 \rho_{\mathrm{s,H_2O}} h_{\mathrm{sl,H_2O}} \frac{\mathrm{d}x}{\mathrm{d}t} \tag{5}$$

Heat transfer by convection is:

$$q_{\mathrm{conv}} = h_{\mathrm{g}} A_{\mathrm{s}} (T_{\mathrm{s,H_2O}} - T_{\infty}) \tag{6}$$

and heat transfer by radiation can be approximated by:

$$q_{\mathrm{rad}} = h_{\mathrm{r}} A_{\mathrm{s}} (T_{\mathrm{s,H_2O}} - T_{\infty}) \tag{7}$$

where

$$h_{\mathrm{r}} = \varepsilon\sigma (T_{\mathrm{s,H_2O}} - T_{\infty})^2 (T_{\mathrm{s,H_2O}} + T_{\infty}) \tag{8}$$

The driving force for water evaporation is the difference between the density of the vapor at the surface and in the air. Heat transfer due to water evaporation is:

$$q_{\mathrm{evap}} = \dot{m}_{\mathrm{evap}} h_{\mathrm{fg,H_2O}} = h_{\mathrm{D}} (\rho_{\mathrm{v,s}} - \rho_{\mathrm{v},\infty}) A_{\mathrm{s}} h_{\mathrm{fg,H_2O}} \tag{9}$$

The mass transfer coefficient, h_{D}, is related to the gas (air) heat transfer coefficient, h_{g}, through Lewis number:

$$\frac{h_{\mathrm{g}}}{h_{\mathrm{D}}} = \rho_{\mathrm{g}} c_{\mathrm{p,g}} \sqrt[3]{\mathrm{Le}^2} \tag{10}$$

Combining eqs. (9) and (10), q_{evap} can be rewritten as:

$$q_{\mathrm{evap}} = \frac{h_{\mathrm{g}} (\rho_{\mathrm{v,s}} - \rho_{\mathrm{v},\infty}) A_{\mathrm{s}} h_{\mathrm{fg,H_2O}}}{\rho_{\mathrm{g}} c_{\mathrm{p,g}} \sqrt[3]{\mathrm{Le}^2}} \tag{11}$$

where

$$\rho_{\mathrm{v,s}} = \frac{P_{\mathrm{sat}} (T_{\mathrm{s,H_2O}})}{R T_{\mathrm{s,H_2O}}} \tag{12}$$

and

$$\rho_{\mathrm{v},\infty} = x_{\mathrm{H_2O}} \frac{P_{\mathrm{sat\ at}\ T_{\infty}}}{R T_{\infty}} \tag{13}$$

The mole fraction for water vapor (*i. e.*, the number of moles of water vapor per number of moles of the mixture of air and water vapor) can be expressed as a function of the absolute humidity and the molar mass for air and water:

$$x_{\mathrm{H_2O}} = \frac{N_{\mathrm{H_2O}}}{N_{\mathrm{mix}}} = \frac{\omega}{\omega + \dfrac{M_{\mathrm{H_2O}}}{M_{\mathrm{air}}}} \tag{14}$$

The absolute humidity in the surrounding air can be determined as follows:

$$\omega = \frac{0.622\varphi P_{\text{sat at } T_\infty}}{P_\infty - \varphi P_{\text{sat at } T_\infty}} \tag{15}$$

The thermal resistors due to conduction, forced convection, radiation, and evaporation heat transfer can be written as:

$$\begin{aligned} R_{\text{cond}} &= \frac{1}{4\pi k_{\text{s,H}_2\text{O}}}\left[\frac{1}{r_\text{o} - x} - \frac{1}{r_\text{o}}\right] \\ R_{\text{conv}} &= \frac{1}{4\pi r_o^2 h_\text{g}} \\ R_{\text{rad}} &= \frac{1}{4\pi r_o^2 h_\text{r}} \\ R_{\text{evap}} &= \frac{\rho_\text{g} c_{\text{p,g}} \sqrt[3]{\text{Le}^2}\,(T_{\text{s,H}_2\text{O}} - T_\infty)}{4\pi r_o^2 h_\text{g} (\rho_{\text{v,s}} - \rho_{\text{v},\infty}) h_{\text{fg,H}_2\text{O}}} \end{aligned} \tag{16}$$

Substituting eq. (16) in eq. (4) and combining with eq. (5), the solidifying water front can be shown to move at the speed:

$$\frac{\text{d}x}{\text{d}t} = \frac{T_{\text{s,H}_2\text{O}} - T_\infty}{\dfrac{\rho_{\text{s,H}_2\text{O}} h_{\text{sl,H}_2\text{O}}}{k_{\text{s,H}_2\text{O}}}(r_\text{o} - x)^2\left[\dfrac{1}{r_\text{o} - x} - \dfrac{1}{r_\text{o}}\right] + \dfrac{(r_\text{o} - x)^2 \rho_{\text{s,H}_2\text{O}} h_{\text{sl,H}_2\text{O}}}{r_\text{o}^2 (h_\text{g} + h_\text{r}) + \dfrac{r_\text{o}^2 h_\text{g} h_{\text{fg,H}_2\text{O}} (\rho_{\text{v,s}} - \rho_{\text{v},\infty})}{\rho_\text{g} c_{\text{p,g}} \sqrt[3]{\text{Le}^2}\,(T_{\text{s,H}_2\text{O}} - T_\infty)}}} \tag{17}$$

The buildup of the liquid water film on the surface of the sphere is function of gravity and water contact angle. The thickness of this film is estimated based on the theory presented by Mikielewicz *et al.* [12]. In the application of water on citrus fruits, the contact angle for water is considered to be 90°, and the minimum thickness needed for the water film before it starts flowing down the surface is estimated from theory [12] to be around 412 μm.

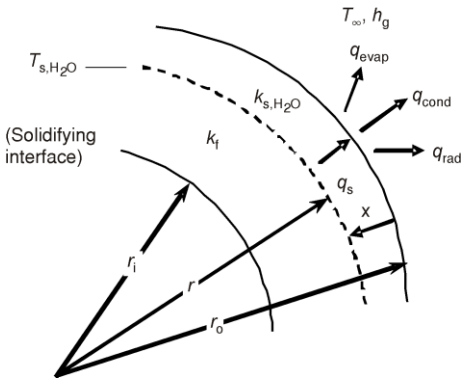

Figure 3. Energy balance on a solidifying water front

Energy equation for the temperature field

A transient conduction heat transfer numerical model is also developed in MATLAB to simulate the cooling of a single *citrus sinensis* fruit for a period that extends from the time water spray on the fruit surface has completely solidified to the time solidification of the juice inside the citrus fruit begins. The model is based on finite difference approach using the implicit method. The sphere consists of two layers: an inner core representing the geometry of

the citrus fruit, and an outer spherical shell representing the ice encasing around the fruit. In this model, the number of nodes used in the radial direction is 35 and that in the circumferential directions is 60. Weighing factors are used to concentrate the grid mesh near the surface. The model's assumptions are:

- a single fruit with perfectly spherical geometry,
- thermal properties are function of temperature only, and are the same in all directions.
- homogeneous boundary conditions along the sphere circumference; also, the speed of the moving ice front is assumed to be the same in all directions,
- ambient conditions such as temperature and wind speed remain constant,
- perfect contact between the water film and the fruit surface,
- infinitely large surroundings compared to the fruit surface,
- effect of the disturbance from the wind on the water film thickness is negligible, and
- dilute spray conditions prevail.

For $T_{s,cs} < T < T_{s,H_2O}$, the governing equation for the temperature in the fruit, T_{cs}, and in the ice, T_{H_2O}, is in the form:

$$\frac{1}{r^2}\frac{\partial}{\partial r}\left(kr^2\frac{\partial T}{\partial r}\right) = \rho c_p \frac{\partial T}{\partial t} \tag{18}$$

The boundary conditions for the temperature field inside the fruit and the ice layer are:

– $r = 0$,

$$k_{cs}\left.\frac{\partial T_{cs}}{\partial r}\right|_{r=0} = 0 \tag{19}$$

– $r = r_i$,

$$k_{cs}\left.\frac{\partial T_{cs}}{\partial r}\right|_{r=r_i} = k_{s,H_2O}\left.\frac{\partial T_{H_2O}}{\partial r}\right|_{r=r_i} \tag{20}$$

– $r = r_o$,

$$-k_{s,H_2O}\left.\frac{\partial T_{H_2O}}{\partial r}\right|_{r=r_o} = (h_g + h_r)(T_{H_2O}|_{r=r_o} - T_\infty) + \frac{h_g(\rho_{v,s}|_{r=r_o} - \rho_{v,\infty})h_{fg,H_2O}}{\rho_g c_{p,g}\sqrt[3]{Le^2}} \tag{21}$$

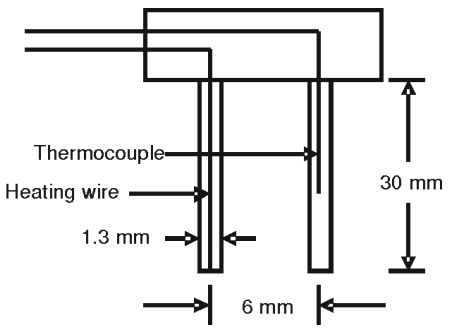

Figure 4. Dual needle heat pulse sensor

Thermal property tests

Experimental studies are conducted to investigate the effect of temperature on the thermal properties (conductivity, thermal diffusivity and specific heat constant) of citrus sinensis. A Dual-Needle Heat-Pulse sensor, KD2 Pro, by Decagon Devices (fig. 4) was used to conduct thermal property analysis [13]. The system consists of two parallel needles that are made of 304 stainless steel material and spaced 6 mm apart. One needle is used as a heating

element subjected to a short duration heating pulse, while the other needle is used for monitoring the temperature. The thermocouple's temperature response to the heat pulse is used to simultaneously determine the thermal conductivity and diffusivity. The volumetric specific heat constant is then determined from these parameters. The uncertainty in the thermal experimental data is ±10%.

Equation (22) is used in curve fitting the temperature time history when the heater is turned on for a duration of t_h, and eq. (23) is used when the heater is turned off:

– for $0 > t < t_h$,

$$T(t) = T_i + \frac{qb_o}{4\pi} t + \frac{qb_1}{4\pi} Ei \frac{b_2}{t} \tag{22}$$

– for $t > t_h$,

$$T(t) = T_i + \frac{qb_o}{4\pi} t + \frac{qb_1}{4\pi} \left(Ei \frac{b_2}{t} - Ei \frac{b_2}{t - t_h} \right) \tag{23}$$

Ei is an exponential integral evaluated using an infinite series [14]:

$$Ei(y) = \gamma + \ln(y) + \sum_{k=1}^{\infty} \frac{y^k}{kk!} \tag{24}$$

where γ is the Euler-Mascheroni constant, and y is a variable. Constants b_o, b_1, and b_2 are calculated using least square procedure. Thermal conductivity and diffusivity are obtained as follows:

$$k_{cs} = \frac{1}{b_1} \tag{25}$$

and

$$\alpha_{cs} = \frac{d^2}{4b_2} \tag{26}$$

The latent heat of fusion of *citrus sinensis* was experimentally determined using a simple Styrofoam calorimeter. 10 g cubes of *citrus sinensis* juice were initially frozen to temperatures below the freezing point for *citrus sinensis*. The experiment was repeated several times for accuracy. In each test, one cubic specimen was inserted into a water bath heated to a temperature slightly above room temperature. Several layers of Styrofoam insulation surrounded the water container from all sides to minimize the heat loss from the water bath to the surroundings. K-type thermocouples, imbedded into the water bath and the cubic specimen, recorded the change in temperatures using a data acquisition device. The latent heat of fusion of *citrus sinensis* was calculated from conservation of energy:

$$h_{sl,cs} = \frac{m_{H_2O}}{m_{cs}} c_{H_2O} (T_{1,H_2O} - T_{2,H_2O}) - c_{cs} (T_{s,cs} - T_{1,cs}) - c_{cs} (T_{2,cs} - T_{s,cs}) \tag{27}$$

Repeated tests show the average value for the latent heat of fusion of *citrus sinensis* juice to be around 262.3 kJ/kg. This is considerably lower than that of pure water (333.7 kJ/kg). Therefore, the amount of heat that needs to be extracted from the *citrus sinensis* fruit for it to solidify is about 79% the amount of energy needed for pure water. Figure 5 shows the

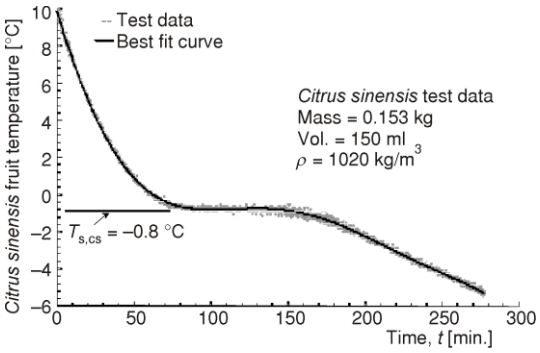

Figure 5. Phase change of citrus fruit during solidification

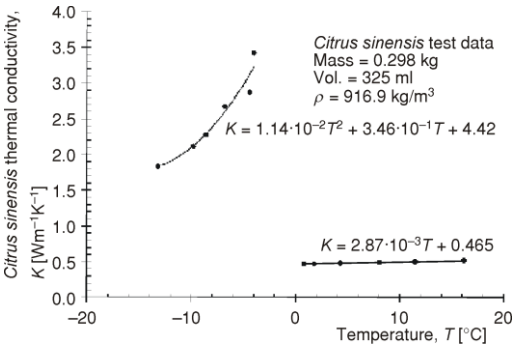

Figure 6. Effect of temperature on thermal conductivity of *citrus sinensis*

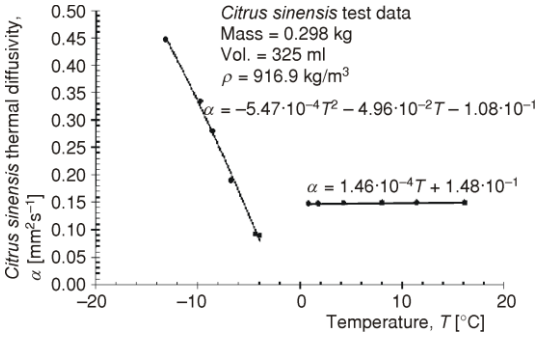

Figure 7. Effect of temperature on thermal diffusivity of *citrus sinensis*

temperature history during the solidification of *citrus sinensis* juice. Solidification is shown to occur around –0.8 °C.

Thermal conductivity, diffusivity, and volumetric specific heat constant for *citrus sinensis* were determined at a wide range of temperatures as shown in figs. 6 through 8. Experimental data in the vicinity of the citrus juice melting point are not available due to the phase change of the state of citrus juice. Direct extrapolation of the thermal properties to the melting point reveals a sharp change in the thermal properties at the melting point. The spike in the thermal conductivity of the *citrus sinensis* juice when it solidifies is accompanied by a strong dependency of thermal conductivity on temperature. Above freezing point, this dependency on temperature is very weak. A similar effect is shown in the experimental data for the volumetric specific heat constant. An opposite effect is shown in the thermal diffisivity data. Thermal diffusivity appears to drop sharply near the freezing point, and increase with further drop in temperature. Above the freezing point, thermal diffusivity is almost constant.

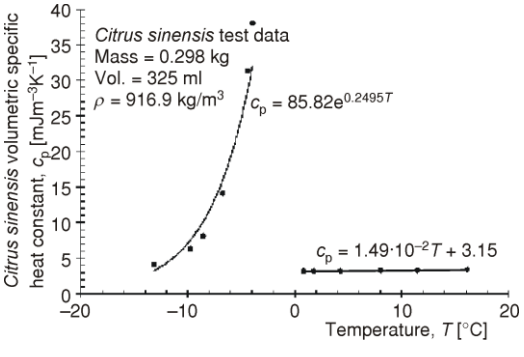

Figure 8. Effect of temperature on specific heat of *citrus sinensis*

Numerical simulations

Simulation results presented in this paper will attempt to portray the sensitivity of the ice buildup around a single citrus fruit as function of time, air speed, and air temperature. In each of the presented cases, the fruit surface is sprayed intermittently with water. During each spray period, incoming water forms a film layer of 412 μm

in thickness around the fruit spherical surface. This is the minimum film thickness needed before water starts flowing down the surface due to gravity [12]. This thickness depends on certain parameters such as the water viscosity, surface tension, contact angle between the water film and the fruit surface, and gravity. In reality, in order to ensure a water film thickness of 412 μm covers the fruit surface uniformly, electrostatic spraying needs to be implemented. In electrostatic spraying, the droplets carry a charge opposite to that of the target surface. Electrostatic spraying distributes the droplets onto the selected target in a controlled and predetermined way, and reduces drift.

Water spray is turned off for a period equal to the time necessary for the water film to freeze on the surface. The freezing time is calculated by integrating eq. (17). As water changes phases from liquid to solid, the temperature inside the fruit will not drop below 0 °C. Furthermore, the fruit will not freeze because the freezing temperature for *citrus sinensis* is experimentally shown to be –0.8 °C. Water from a spraying system can intermittently spray on and off to maintain the fruit surface temperature above the fruit freezing temperature. Figures 9 and 10 show the time history of ice sheet thickness for air speeds of 1 and 5 m/s, and for air temperatures of –1, –5, and –10 °C. Each data point in these plots corresponds to a

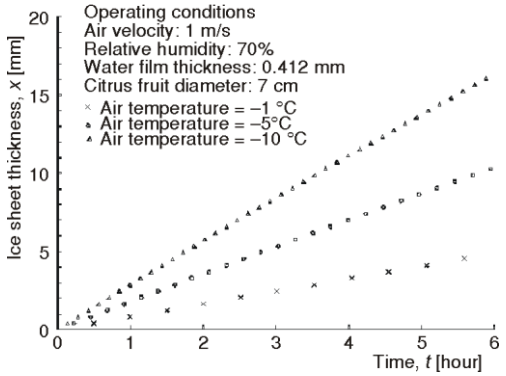

Figure 9. Ice sheet thickness *vs.* time (1 m/s air speed

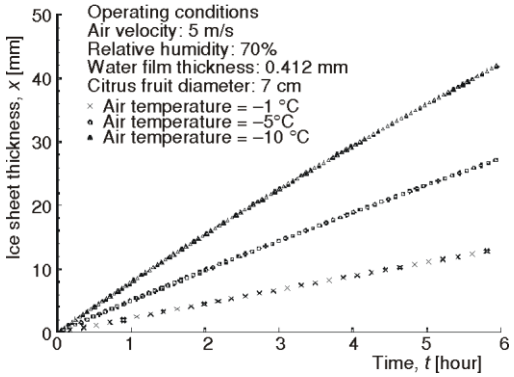

Figure 10. Ice sheet thickness *vs.* time (5 m/s air speed)

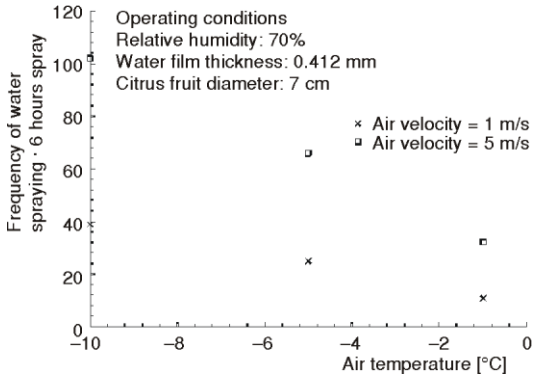

Figure 11. Effect of operating conditions on spray frequency

water film layer that is 412 μm in thickness. The separation between the data points on the time axis corresponds to the period water spraying is turned off. The figures also show the colder the air temperature and the higher air speed, the quicker the water film solidifies on the fruit surface. Figure 11 shows the frequency of water spraying increases with the decrease in air temperature and increase in air speed.

Water spraying of fruits cannot continue indefinitely because at a certain instant in time the additional weight from the ice buildup on the fruit surface can

cause damage to the fruit. Figures 12 and 13 show simulation runs for the fruit surface temperature when water spraying is intermittently turned ON and OFF. In fig. 12 the spray frequency is 1.83 cycles per hour, while in fig. 13 the spray frequency is 5.3 cycles per hour. Figures 12 and 13 also show simulation runs for the fruit surface temperature from the time sprays are permanently turned off to the time the fruit surface reaches the freezing temperature of –0.8 °C. This is done by numerically integrating eq. (18) subject to the boundary conditions of eq. (19) through (21) for the citrus core and the ice shell. Figures 12 and 13 present the results for air temperatures of –1 and –5 °C, respectively, and ice sheet thicknesses of 1 and 5 mm. A case run where no water is sprayed on the fruit is also shown.

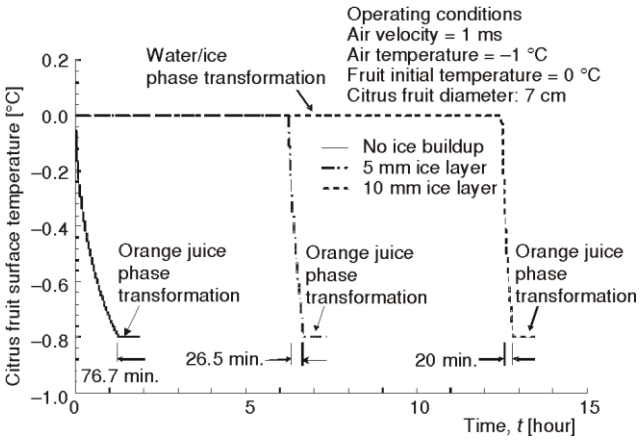

Figure 12. Time history of the citrus fruit surface temperature during and after spraying (T_∞ = –1 °C)

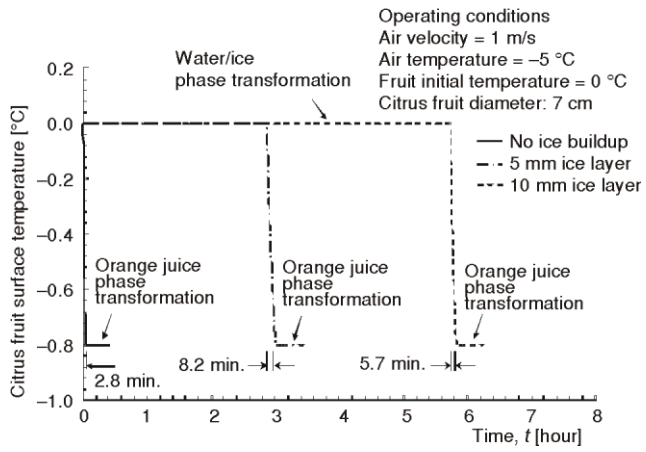

Figure 13. Time history of the citrus fruit surface temperature during and after spraying (T_∞ = –5 °C)

Figure 12 shows when water is intermittently sprayed on the fruit surface, the time required for a 5 mm ice layer to develop is 6.25 hours, and that required for a 10 mm ice layer to develop is 12.5 hours. During this period, the fruit surface temperature remains protected at 0 °C which is above the freezing temperature of the fruit. In fig. 13, the time required for a 5 mm ice layer to develop is 2.87 hours. For the development of 10 mm ice layer, the required time is 5.73 hours. For the same ice layer thickness to develop, the cooler the ambient the less amount of time the fruit has before freezing.

The simulations in figs. 12 and 13 also show when spraying is turned off permanently, the presence of the ice sheet adds only few more minutes of protection time to the fruit before the fruit drops to the freezing temperature (–0.8 °C). For the case when the air temperature is –1 °C (fig. 12), the presence of 5 mm and 10 mm ice layers result in 26.5 min. and 20 min., respectively, of additional protective time if water spraying stops permanently. If no ice layer is present on the fruit surface, this protective time is 76.7 min. For the case when the air temperature is –5 °C (fig. 13), the presence of 5 mm and 10 mm ice layers result in 8.2 min. and 5.7 min., respectively, of additional protective time if

water spraying stops permanently. If no ice is present at this ambient temperature, the protective time is 2.8 min. only.

In the simulations presented, the amount of water required during each spray cycle is about 6.4 ml per fruit. This volume provides a water film thickness of 412 μm on a citrus fruit surface with a diameter of 7 cm. In this study, simulations were performed on a single citrus fruit. In reality a bundle of fruits will be present on the tree and all will be sprayed at the same time. The model assumes the water to be sprayed uniformly over the fruit surface. This is difficult to achieve since the nozzles may be positioned in one location with respect to the fruits unless electrostatic spraying is used. Also, the model considers the effect of only the surface tension and gravity in the development of the water film thickness, and assumes the effect of any external disturbance to be negligible. In reality any external disturbance such as that of wind will cause water to drip from one fruit surface to the other. Therefore the amount of water used for spraying a single citrus fruit in this study should be considered as an upper bound limit especially for conditions where wind speed is high.

Conclusions

A numerical model was developed to simulate the frost protection of a single citrus fruit using water from a spray system. The model simulates the movement of the solidifying water front as the ice sheet encases the fruit. Simulations were conducted to evaluate the effect of air temperature, air speed, radiation and water film evaporation on the development of the ice layer. Simulations show the colder the air temperature and the higher the air speed, the quicker the water film solidifies on the fruit surface. As a result, the frequency of water spraying increases with the decrease in air temperature and increase in air speed. Simulations show when water spray is turned off, the presence of the ice sheet adds few minutes of protective time before the fruit temperature drops to the fruit freezing point. Tests were conducted to determine the effect ambient temperature has on the fruit thermal conductivity, diffusivity, and specific heat constant. Direct extrapolation of the thermal properties to the fruit freezing temperature reveals a sharp change in the thermal properties at the freezing point.

Nomenclature

A_s – sphere surface area, [m^2]
b_o, b_1, b_2 – constants for least square procedure
c – specific heat, [$Jkg^{-1}K^{-1}$]
c_p – specific heat at constant pressure, [$Jkg^{-1}K^{-1}$]
d – distance between needles for heat sensor
D_o – sphere outer diameter, [m]
Ei – exponential integral
h_D – mass transfer coefficient, [ms^{-1}]
h_{fg} – latent heat of vaporization, [Jkg^{-1}]
h_g – air heat transfer coefficient, [$Wm^{-2}K^{-1}$]
h_r – radiation heat transfer coefficient, [$Wm^{-2}K^{-1}$]
h_{sl} – latent heat of fusion, [Jkg^{-1}]
k – thermal conductivity, [$Wm^{-1}K^{-1}$]
Le – Lewis number
M – molecular mass, [$kgkmol^{-1}$]
m – mass, [kg]
$\dot{m}$ – mass flow rate, [kgs^{-1}]
N – number of moles, [kmol]
Nu – Nusselt number
P – total pressure, [Nm^{-2}]
q – heat transfer, [W]
R – thermal resistor, [$°CW^{-1}$]
r – radial location in the sphere, [m]
Re – Reynolds number
T – temperature, [°C]
T_∞ – air temperature, [°C]
t – time, [s]
t_h – pulse heater duration time, [s]
U_g – air speed, [ms^{-1}]
x – ice shell thickness, [m]
x_{H_2O} – mole fraction for water vapor

Greek symbols

α – thermal diffusivity, [m^2s^{-1}]
γ – Euler-Mascheroni constant
ε – surface emissivity
θ – angular position from stagnation point, [deg.]
ν_g – air kinematic viscosity, [m^2s^{-1}]
ρ – density [kgm^{-3}]
$\rho_{v,s}$ – vapor density at the surface, [kgm^{-3}]
$\rho_{v,\infty}$ – vapor density in air, [kgm^{-3}]
σ – Stefan-Boltzmann constant, [$Wm^{-2}K^{-4}$]
φ – relative humidity
ω – absolute humidity

Subscripts

cond – conduction heat transfer
conv – convection heat transfer
cs – *citrus sinensis*
evap – evaporation
f – fluid (liquid)
g – gas (air)
i – inner
o – outer
rad – radiation heat transfer
s – solid (ice)
sat – saturation vapor
1 – initial
2 – final

References

[1] Lengerke, H. J. von, On the Short-Term Predictability of Frost and Frost Protection – A Case Study on Dunsandle Tea Estate in the Nilgiris (South India), *Agricultural Meteorology*, *19* (1978), 1, pp. 1-10
[2] Hamer, P. J. C., An Automatic Sprinkler System Giving Variable Irrigation Rates Matched to Measured Frost Protection Needs, *Agricultural Meteorology*, *21* (1980), 4, pp. 281-293
[3] Hamer, P. J. C., The Heat Balance of Apple Buds and Blossoms. Part II – The Water Requirements for Frost Protection by Overhead Sprinkler Irrigation, *Agricultural and Frost Meteorology*, 37 (1986), 2, pp. 159-174
[4] Hamer, P. J. C., Simulation of the Effects of Environmental Variables on the Water Requirements for Frost Protection by Overhead Sprinkler Irrigation, *Journal of Agricultural Engineering Research*, *42* (1989), 2, pp. 63-75
[5] Edling, R. J., Constantin, R. J., Bourgeois, W. J., Louisiana Citrus Frost Protection with Enclosures and Microsprinklers, *Agricultural and Forest Meteorology*, *60* (1992), 1-2, pp. 101-110
[6] Anconelli, S., *et al*., Micrometeorological Test of Microsprinklers for Frost Protection of Fruit Orchards in Northern Italy, *Physics and Chemistry of the Earth*, *27* (2002), 23-24, pp. 1103-1107
[7] Ghaemi, A. A., Rafiee, M. R., Sepaskhah, A. R., Tree-Temperature Monitoring for Frost Protection of Orchards in Semi-Arid Regions Using Sprinkler Irrigation, *Agricultural Sciences in China*, *8* (2009), 1, pp. 98-107
[8] Stombaugh, T. S., *et al.*, Automation of a Pulsed Irrigation System for Frost Protection of Strawberries, *Applied Engineering in Agriculture*, *8* (1992), 5, pp. 597-602
[9] Zhitkevich, L. K., Simchenko, L. E., Investigation of Local and Average Heat Transfer between a Sphere and an Airstream, *Journal of Engineering Physics and Thermophysics*, *11* (1966), 1, pp. 7-9
[10] Cary, J. R., The Determination of Local Forced Convection Coefficients for Spheres, *Transactions of the American Society of Mechanical Engineers*, *75* (1953), 4, pp. 483-487
[11] Wadsworth, J., The Experimental Examination of the Local Heat Transfer on the Surface of a Sphere when Subjected to Forced Convective Cooling, Report No. MT-39, National Research Council of Canada, Ottawa, Ont., Canada, 1958
[12] Mikielewicz, J., Moszynski, J. R., Minimum Thickness of a Liquid Film Flowing Vertically Down a Solid Surface, *International Journal of Heat and Mass Transfer*, *19* (1976), 7, pp. 771-776
[13] KD2 Pro Operator's Manual, Version 8, Decagon Devices, Pullman, Wash., USA, 2010
[14] Abramowitz, M, Stegun, I. A., Handbook of Mathematical Functions, Dover Publications, Inc., New York, USA, 1972

Paper submitted: March 31, 2011
Paper revised: August 9, 2011
Paper accepted: August 11, 2011